University of Baghdad
College of Engineering
JOURNAL OF ENGINEERING

Journal of Engineering

journal homepage: www.jcoeng.edu.iq

Volume 32 Number 9 September 2026

Numerical Investigation of the Thermal Performance of a Double-Pass Counter-Flow Flat-Plate Solar Air Collector Based on the Taguchi Method

Hussein Muwafaq M. Ali [1, *], **Oday Ibraheem Abdullah** [1, 2, 3], **Hussein K. Jobair** [1]

[1] Department of Energy Engineering, College of Engineering, University of Baghdad, Baghdad, Iraq
[2] Mechanical Engineering Department, College of Engineering, Gulf University, Sanad, Bahrain
[3] Petroleum Engineering Department, College of Engineering, Al-Naji University, Baghdad, Iraq

ABSTRACT

Solar air collectors have been widely used in industries and agriculture because of their structural simplicity and economic feasibility. Still, their thermal performance characteristics are constrained by insufficient convective thermal exchange between the absorbing surface and the airflow. In this study, a numerical investigation and optimization of the thermal performance characteristics of the double-pass counter-flow flat-plate solar air collector are carried out using the CFD–Taguchi method. The heat and airflow under forced convection conditions have been modeled in ANSYS using a three-dimensional steady-state (CFD) model. Key factors such as mass flow rate (0.01–0.07–0.15 kg/s), channel height configurations, and material properties (copper, aluminum, and steel) have been studied. Using Taguchi analysis and ANOVA technique, an optimal combination of the parameters to enhance the thermal characteristics has been obtained. The simulation results reveal that the maximum efficiency attained is 0.531, where mass flow rate was found to be the predominant parameter accounting for 99.46% of total effects. Higher efficiency can be achieved with increased flow rate as a result of higher convection process; however, an increase in the mass flow rate decreases air outlet temperature because of a shorter exposure period. The effect of channel height and material was very small (less than 0.2%). The theoretical model has been checked using literature data; the largest error was 6.65%. From this study, it can be noticed that focusing on proper airflow management is more important than proper material selection.

Keywords: Absorber material, CFD, Solar air collector, Taguchi method, Thermal efficiency.

1. INTRODUCTION

Solar air heaters (SAHs) find extensive application in industries and agriculture owing to their easy-to-assemble nature and economic operating costs **(Saini et al., 2007)**. Yet, their thermal effectiveness is constrained by the low convective heat transfer rate from the absorber wall to the airflow. To improve this situation, many research efforts have been

*Corresponding author
Peer review under the responsibility of University of Baghdad.
https://doi.org/10.31026/j.eng.2026.09.03

Article received: 23/05/2026
Article revised: 26/07/2026
Article accepted: 06/08/2026
Article published: 01/09/2026

conducted to increase heat transfer through the internal modification of the airflow duct **(Panda and Kumar, 2021)**.

Another one of the earliest techniques used for improving convective heat transfer by modifying the flow internally is artificial roughness creation, in which rib-like, baffled, and fin-like shapes were created to cause turbulence and disturb the thermal boundary layer and thus improve heat transfer. Another approach used at an earlier stage to improve heat transfer was modification in absorber design, such as using porous or volume absorbers in certain experiments, as described by **(Ramani et al., 2010)** studied the effect of double-pass solar air collectors with a porous absorbent medium, wherein they found out that the enhanced heat transfer surface area resulted in improved thermal efficiency of 25%. In a three-dimensional CFD analysis of staggered cuboid baffles, **(Parsa et al., 2021)** proved that optimization of geometric parameters could result in thermohydraulic performance enhancement of up to 17.5%. Additionally, **(Choi and Choi, 2020)** observed that transverse triangular blocks result in an increase of up to 3.37 times the Nusselt number relative to smooth ducts. In further research on configurations based on obstacles, the effect of flow-induced turbulence on heat transfer has been emphasized. Specifically, **(Alam and Kim, 2016)** studied obstacles having semi-ellipse geometry and determined that the heat transfer was greatly enhanced through staggering of blocks and at an angle of attack equal to 75°. Similar observations were made by **(Singh et al., 2015)**, who observed substantial heat transfer augmentation through the use of non-uniform transverse ribs, with an enhancement of the Nusselt number up to 1.78 times but with associated higher losses in terms of frictional forces. The latest developments concern numerical simulations for internal geometry optimizations. For instance, **(Nagaraj et al., 2022)** optimized aerofoil-shaped fins through a combination of experiments and simulations, resulting in a heat transfer enhancement of up to 23.24%. In addition, **(Hamad et al., 2023)** studied trapezoidal rib configurations and reported heat transfer enhancements of approximately 2.01 times compared to smooth ducts. More recently, **(Hussein et al., 2023)** introduced a novel tubular absorber design for double-pass solar air heaters, demonstrating significant improvement in effective efficiency, reaching a maximum of 80.9% due to increased heat transfer surface area.

Many researchers have focused on improving the thermal performance of solar air collectors using artificial roughness elements and modified absorber surfaces. Early studies investigated transverse ribs and wedge-shaped roughness to enhance convective heat transfer by disturbing the thermal boundary layer **(Sahu and Bhagoria, 2005; Karwa et al., 1999; Layek et al., 2007; Hans et al., 2010)**. Later investigations introduced additional roughness configurations, including protruding and curved elements, and reported further improvements in heat transfer performance **(Yadav and Bhagoria, 2013; Yadav and Kaushal, 2013; Patel et al., 2020; Srivastava et al., 2020)**. More recent studies have continued to optimize roughness geometries and absorber surfaces using advanced designs and numerical approaches **(Chand et al., 2022; Gupta et al., 1993; Misra et al., 2020; Gill et al., 2021)**. Furthermore, computational fluid dynamics and optimization techniques have been widely adopted to investigate finned absorbers, hybrid roughness configurations, and innovative rib geometries, providing further improvements in the thermal performance of solar air collectors **(Bhagoria et al., 2002; Aharwal et al., 2009; Saravanan et al., 2021; Kumar et al., 2023)**. Additional numerical investigations have also demonstrated the effectiveness of artificial roughness under different operating conditions **(Prasad and Mullick, 1983; Saini and Saini, 2008; Haldar et al., 2022; Singh and Singh, 2018).**

Although extensive research has been conducted on solar air collectors, previous studies have primarily focused on improving thermal performance through artificial roughness elements, fins, baffles, and absorber geometry modifications. While computational fluid dynamics (CFD) and Taguchi optimization have been widely used to evaluate performance, insufficient attention has been paid to assessing the relative impact of operating parameters and absorber plate materials in double-pass counter flow flat-plate solar air collectors under identical operating conditions. Furthermore, the comparative impact of commonly used metallic absorber materials, copper, aluminum, and steel, has not been comprehensively evaluated within an integrated framework combining computational fluid dynamics, Taguchi optimization, and analysis of variance (ANOVA). Consequently, the relative importance of these design and operational parameters remains insufficiently understood, representing a research gap addressed by this study.
Accordingly, this study develops a 3D computational fluid dynamics model in ANSYS software to investigate the thermal performance of a double-pass counterflow solar air collector with flat plates. The effects of channel height, air mass flow rate, and absorber plate material are systematically evaluated under identical operating conditions. The Taguchi method, combined with analysis of variance (ANOVA), is used not only to determine the optimal operating conditions but also to determine the statistical contribution of each parameter to the collector's thermal efficiency. The results provide practical engineering guidance for prioritizing parameters that most effectively improve collector performance, while also assessing whether the choice of absorber material leads to a significant improvement in thermal efficiency.

2. NUMERICAL METHOD

2.1 Governing Equations

The numerical analysis of the solar air heater is based on the solution of the governing conservation equations for mass, momentum, and energy. The airflow is assumed steady, incompressible, and three-dimensional. The useful heat gain and thermal efficiency of the collector are then calculated from the outlet air temperature obtained from the simulation.

1. The continuity equation can be written as follows **(Bisnovatyi-Kogan and Lovelace, 2001)**:

$$\nabla \cdot \vec{u} = 0 \tag{1}$$

where, the $\vec{u}$ is the fluid velocity vector, and ∇ is the vector differential operator (del operator). This equation represents the conservation of mass for incompressible airflow inside the solar collector.

2.The Momentum equations **(Batchelor and Batchelor, 1967)**:

$$\nabla \cdot (\rho\vec{u}\vec{u}) = -\nabla p + \nabla \cdot (\bar{\bar{\tau}}) \tag{2}$$

This equation represents the conservation of incompressible momentum for airflow. The $\vec{u}$ is the fluid velocity vector, ρ is the air density, and p is the static pressure. The term $\nabla \cdot (\rho\vec{u}\vec{u})$ denotes the convective transport of momentum, $-\nabla p$ represents the pressure gradient force, and $\nabla \cdot (\bar{\bar{\tau}})$ accounts for the viscous stresses within the fluid. In this configuration, the additional body force term and the gravitational force are neglected, i.e., $\vec{F}$=0 and $\vec{g}$=0. The stress tensor, $\bar{\bar{\tau}}$, is related to the strain-rate tensor by

$$\tau = \mu \left(\nabla \vec{u} + (\nabla \vec{u})^T - \frac{2}{3} \delta \, \nabla \cdot \vec{u} \right) \quad (3)$$

Where τ is the viscous stress tensor, μ is the dynamic viscosity, $\vec{u}$ is the velocity vector, δ is the Kronecker delta (unit tensor), and $\nabla \cdot \vec{u}$ represents the volumetric deformation rate. The first two terms account for shear deformation, while the last term represents volumetric dilation and vanishes for incompressible flow.

3.The Energy equation **(Arpaci and Larsen, 1984)**:

$$\nabla \cdot \left(\vec{u}(\rho E + p) \right) = \nabla \cdot (k \nabla T) + \nabla \cdot (\tau \cdot \vec{u}) \quad (4)$$

where E is the total energy (J/kg), k is the thermal conductivity (W/m·k), T is the temperature (K), ρ is the air density (kg/m^3), p is the static pressure (Pa), $\vec{u}$ is the fluid velocity vector (m/s), and τ is the viscous stress tensor (Pa).

2.2 Realizable k–ϵ Model

The turbulent flow inside the solar air heater is modeled using the realizable k–ε turbulence model, which is widely used for internal flow applications due to its robustness and accuracy. The model solves two additional transport equations for the turbulent kinetic energy k and its dissipation rate ε, which are expressed as follows **(Shaheed et al., 2019)**:

$$\frac{\partial}{\partial t}(\rho k) + \nabla \cdot (\rho k \vec{v}) = \nabla \cdot \left[\left(\mu + \frac{\mu_t}{\sigma_k} \right) k \right] + G_k - \rho \varepsilon \quad (5)$$

where k is the turbulent kinetic energy (m^2/s^2), G_k is the production of turbulent kinetic energy due to the mean velocity gradients, ρ is the air density (kg/m^3), μ is the dynamic viscosity (kg/m·s), μ_t is the turbulent viscosity (kg/m·s), and σ_k is the turbulent Prandtl number for the turbulent kinetic energy.

$$\frac{\partial}{\partial t}(\rho \varepsilon) + \nabla \cdot (\rho \varepsilon \vec{v}) = \nabla \cdot \left[\left(\mu + \frac{\mu_t}{\sigma_\varepsilon} \right) \varepsilon \right] + \rho C_1 S_\varepsilon - \rho C_2 \frac{\varepsilon^2}{k + \sqrt{v\varepsilon}} \quad (6)$$

where ε is the turbulent dissipation rate (m^2/s^3), C_1 and C_2 are empirical model constants, S_ε is a source term in the realizable **k–ϵ** model, $\vec{v}$ is the kinematic viscosity (m^2/s), μ is the dynamic viscosity (kg/m·s), μ_t is the turbulent viscosity (kg/m·s), and σ_k is the turbulent Prandtl number for the turbulent dissipation rate.

2.3 Mesh Independence Test

Mesh independence analysis is conducted to verify the independence of the solution from the number of mesh elements. This is done by analyzing several meshes having varying degrees of element concentration under identical operating conditions. It is found that the variation in the outlet temperature becomes negligible beyond a certain element concentration level. Thus, the mesh used has a total of around 2,469,635 elements, as illustrated in **Fig. 1**. The maximum mesh skewness was maintained below 0.9. Five inflation layers with a growth rate of 1.2 were applied near the walls. The realizable k–ε turbulence model with standard wall functions was employed. The area-weighted average wall y+ was approximately 4.14. The maximum number of iterations was set to 500. Convergence was achieved when the residuals reached 10^{-3} for continuity, momentum, turbulent kinetic energy, and turbulence dissipation rate, and 10^{-6} for the energy equation.

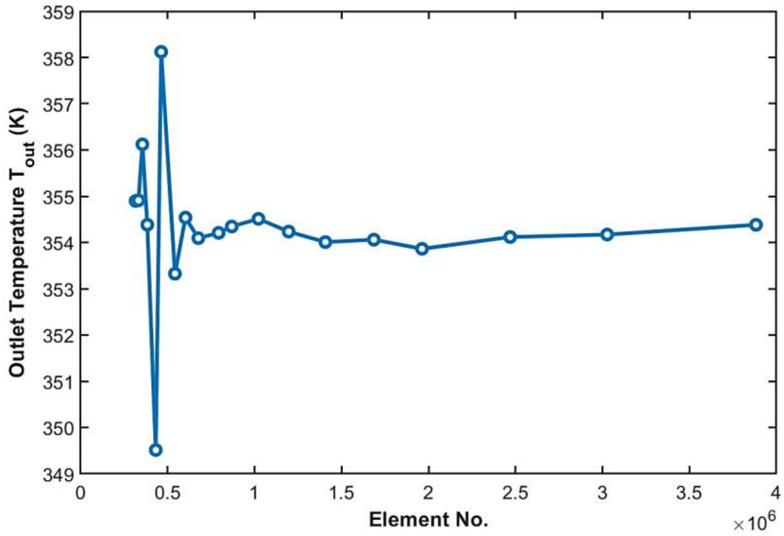

Figure 1. Grid independence test

2.4 Model Validation

The developed computational fluid dynamics (CFD) model has been verified through comparison with previously reported results under the same geometry and operating conditions **(Jobair and Nima, 2025)**. Verification is carried out based on the comparison of the useful heat gain prediction. Percentage deviation between the current results and the reference data is computed using the following equation:

$$Error(\%) = \left| \frac{Q_{u,Present} - Q_{u,ref}}{Q_{u,Present}} \right| \times 100 \quad (7)$$

where $Q_{u,Present}$ is the useful heat gain predicted by the present numerical model (W), and $Q_{u,ref}$ is the useful heat gain reported in the reference study (W). It has been found that there is a deviation of 6.65%, which falls within the acceptable range of accuracy reported in solar air heater analysis using CFD modeling. This implies that the developed numerical model is valid and reliable, as presented in **Fig. 2**.

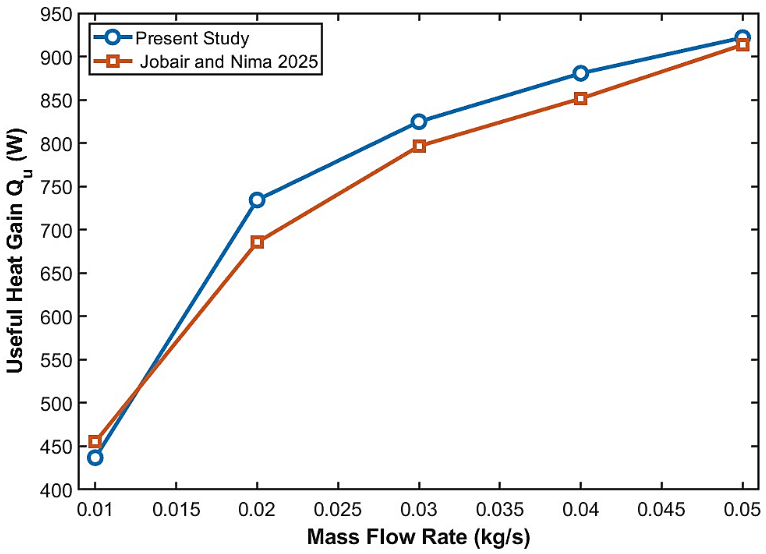

Figure 2. Validation of the developed numerical model

2.5 Case Study

In this study, a Double-Pass Counter-Flow Solar Air Heater (DCSAH) is studied for its application in industry. The dimensions of the collector are 2020mm in length and 1000mm in width to give a sufficiently large absorber area. The length of the absorber plate is 2000mm, which ensures uniform heat absorption in the flow direction. The collector setup utilizes conventional flat absorber plates evaluated across three different materials: copper, aluminum, and steel, as shown in **Fig. 3**. Ambient air enters the collector from the inlet, flows along the upper channel through the glass cover and the absorber plate, turns around, passes through an air gap, and then flows into the lower channel. The boundary conditions for the SAH provided with an absorber plate are depicted in **Fig. 4**. The collector geometry and orientation are defined according to typical design parameters reported in the literature. **Table 1** summarizes the general specifications of the DCSAH. The collector is tilted at 33.3° and oriented southward to represent realistic operating conditions for the Baghdad climate. A single glass cover is considered in the numerical model to account for solar radiation transmission and convective heat losses to the ambient.

Table 1. Design parameters of the double-pass solar air collector with a flat absorber plate.

Specifications	Symbol	Value
Length of collector (mm), flat	L_T	2020
Length of absorber plate (mm)	L_a	2000
Width of collector (mm)	W	1000
Upper and lower channel height (mm)	h	50,50
		70,30
		30,70
Air gap (mm), flat	g_a	20

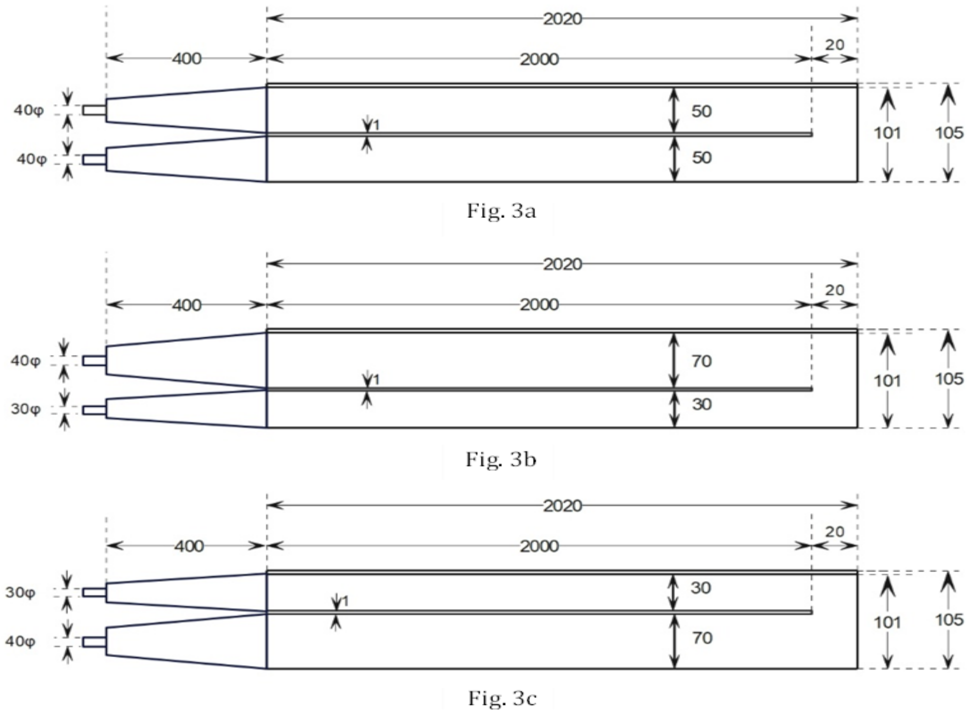

Figure 3. Double-pass SAHs characteristics: schematic drawing of the DCSAH with a flat absorber plate and dimensions. a) h=50,50, b) h=70,30, c) h=30,70.

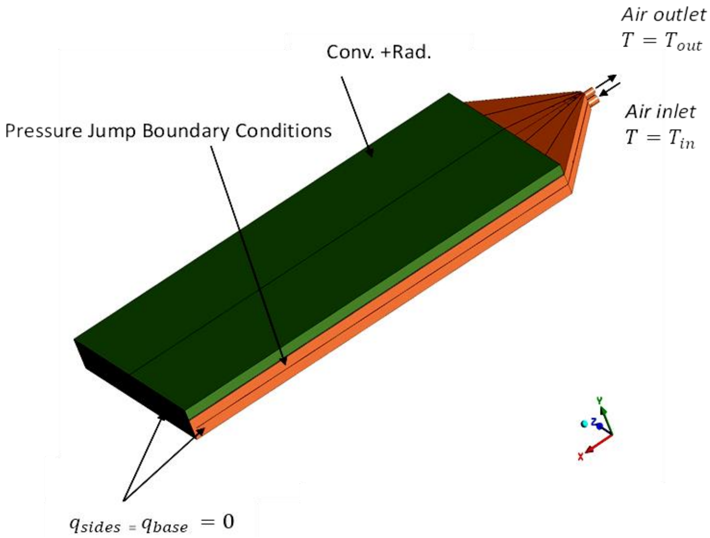

Figure 4. Boundary conditions of the system

The back and side walls of the collector are thermally insulated in the simulation to minimize heat losses, allowing the analysis to focus on the heat transfer within the air channels and absorber plate. The boundary conditions applied to the solar air heater are defined as follows. The boundary conditions applied to the solar air heater include a uniform inlet velocity with a constant temperature at the inlet and a pressure outlet condition with zero-gauge pressure at the outlet. A constant heat flux is imposed on the absorber plate to simulate solar irradiation. The top glass cover is modeled using a convective heat transfer boundary condition with the ambient environment, while the side and bottom walls are assumed to be adiabatic. In addition, a no-slip boundary condition is applied at all solid surfaces. The overall methodology of the present study is illustrated in **Fig. 5**. In the present CFD model, a constant heat flux corresponding to a solar radiation intensity of 880 W/m^2 was applied, while radiative heat transfer was not explicitly considered. This approach is commonly adopted in parametric studies to ensure controlled comparison between cases, although it may limit the exact representation of real operating conditions. The simulation was performed during clear sky conditions in Baghdad, Iraq, at 11:00 am on June 16.

3. RESULTS AND DISCUSSION

This section presents and discusses the numerical results obtained from the CFD simulations based on the Taguchi analysis. The effects of channel height, air mass flow rate, and absorber plate material on the thermal efficiency of solar air collector are systematically evaluated. The results are interpreted using temperature contour distributions, Taguchi main effects plots, signal-to-noise (S/N) analysis, ANOVA, and regression analysis to identify the dominant parameters governing the collector thermal performance. To find the optimal values for each operational factor suggested in this work to obtain the optimal thermal efficiency.

According to the results obtained from the Taguchi analysis, two extremities were chosen for further visualization through ANSYS software, as shown in **Table 2**. Case 9 is considered the case that has the maximum thermal efficiency value, while Case 4 is the one that gives the minimum efficiency value. These cases were analyzed to illustrate the differences in the temperature distribution and heat transfer characteristics of the solar air collector under the best and worst operating conditions, as shown in **Figs. 6 and 7**.

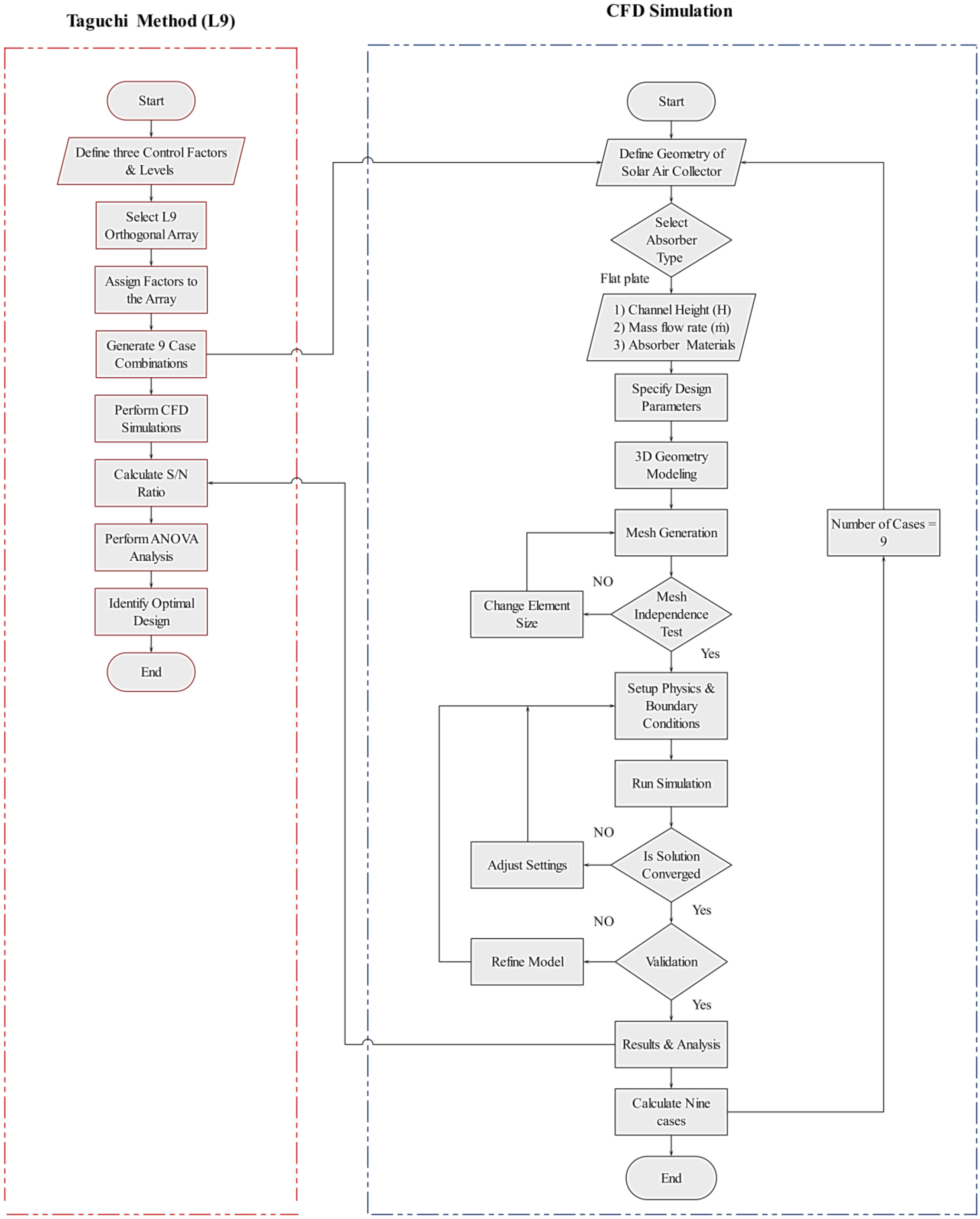

Figure 5. Flow chart of CFD modeling and Taguchi optimization.

The temperature contours provide a qualitative visualization of the heat transfer process and clearly demonstrate the influence of operating conditions on the thermal behavior of the collector. **Fig. 6** shows that the low mass flow rate results in a less uniform temperature distribution and lower heat removal from the absorber plate, leading to reduced thermal efficiency. In contrast, **Fig. 7** exhibits a more effective heat transfer process under the optimum operating conditions. The higher mass flow rate enhances convective heat transfer, resulting in improved heat removal and consequently higher thermal efficiency.

Table 2. Taguchi L9 design with their respective thermal efficiency values.

Exp. No	A (High)	B (Flow Rate)	C (Material)	Thermal efficiency (η)
1	Low 30,70	Low 0.01	Aluminum1	0.27915
2	Low 30,70	Medium 0.07	Copper2	0.47685
3	Low 30,70	High 0.15	Steel3	0.51066
4	Medium 50,50	Low 0.01	Copper2	0.26980
5	Medium 50,50	Medium 0.07	Steel3	0.49718
6	Medium 50,50	High 0.15	Aluminum1	0.51049
7	High 70,30	Low 0.01	Steel3	0.28109
8	High 70,30	Medium 0.07	Aluminum1	0.48521
9	High 70,30	High 0.15	Copper2	0.53112

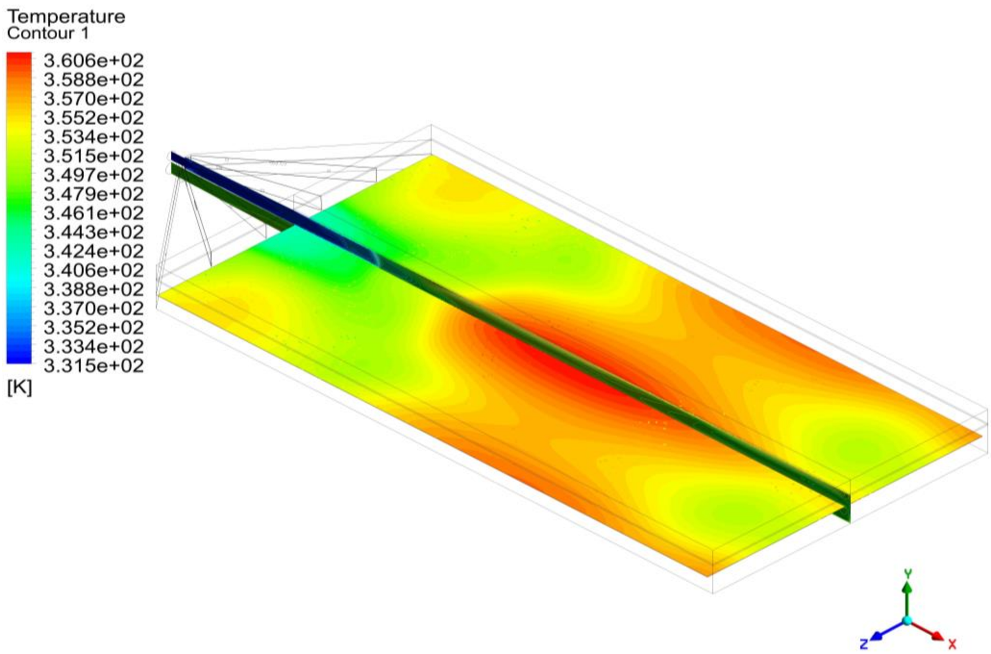

Figure 6. Temperature contours for the lowest (Case 4) thermal efficiency cases.

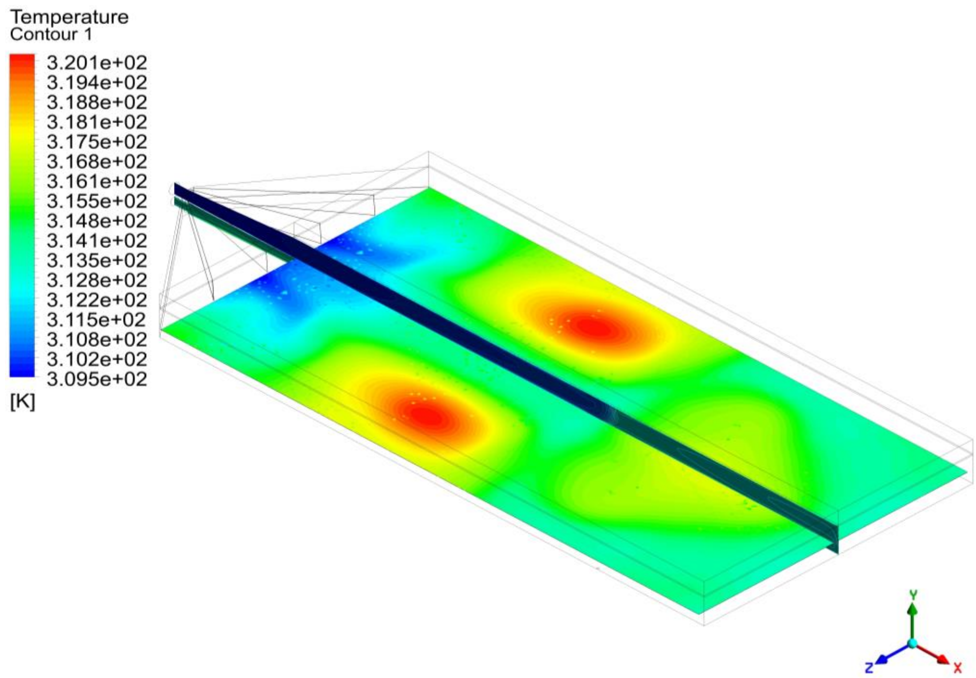

Figure 7. Temperature contours for the highest (Case 9) thermal efficiency cases.

As shown in **Fig. 8**, there is an obvious indication that the mass flow rate is the most influential parameter affecting the response variable. The graph shows a strong positive relationship, whereby the mean value increases significantly when the flow rate increases from 0.01 to 0.15 kg/s. Therefore, it shows that the mass flow rate has a significant influence on the system performance. On the other hand, the channel height (high) and the absorber material show almost a flat trend for all the levels.

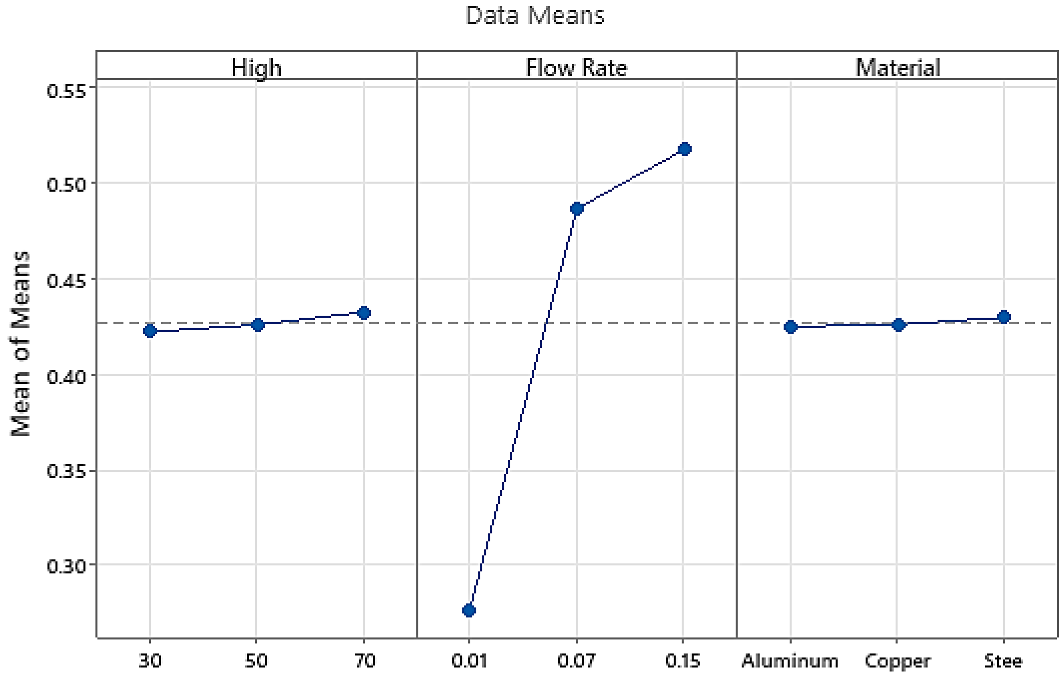

Figure 8. Main effects plot for means

Thus, it shows that the two variables have low sensitivity in terms of their influence on the response variable. In this case, it shows that their influence on the system performance is relatively low compared to the effect of the mass flow rate. The increase in thermal efficiency with increasing mass flow rate is attributed to the enhancement of convective heat transfer caused by the higher air velocity. Although increasing the flow rate reduces the air residence time inside the collector, the improvement in convective heat transfer outweighs this effect, resulting in an overall increase in thermal efficiency.

From **Fig. 9**, it is clear that mass flow rate is the critical factor influencing the process stability and robustness. The S/N ratio shows a sharp increase with an increase in the flow rate from 0.01 to 0.15 kg/s, with the ratios increasing from approximately −11 to −5.7. This sharp increase demonstrates the decrease in variability and the move towards robustness in the process. On the other hand, factors such as high channel height and absorber material show a negligible impact on the S/N ratio as their responses remain almost constant within their respective levels. This implies that their impact on the robustness of the process is minimal, thus making them secondary factors. They should therefore be chosen according to convenience for reasons like cost-effectiveness without affecting the system performance.

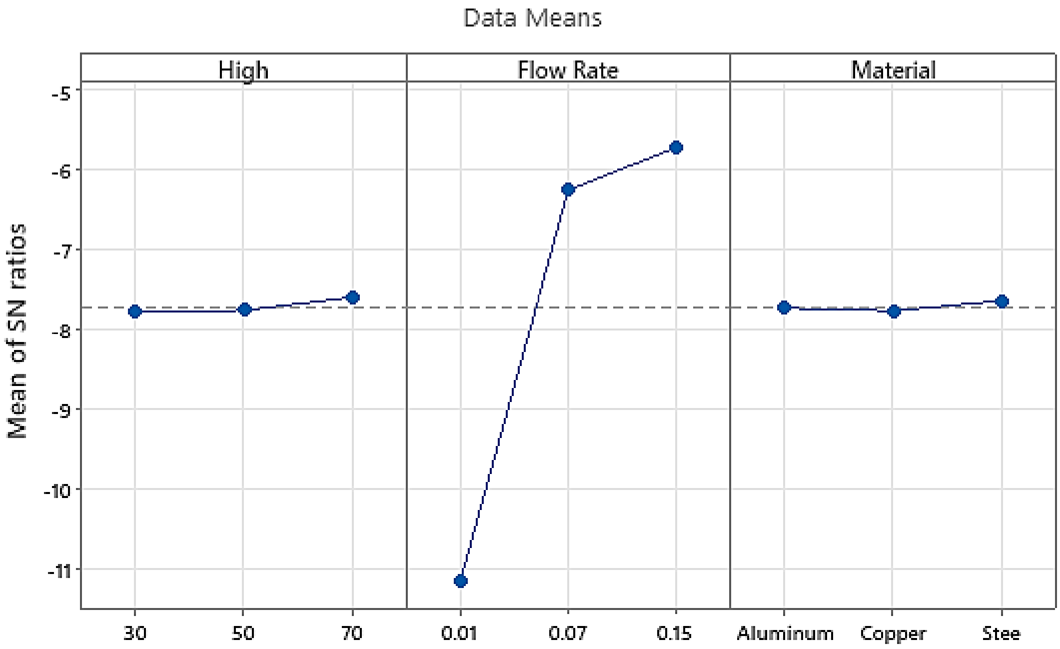

Figure 9. Main effects plot for signal-to-noise (SN) ratios (Larger is Better)

From the ANOVA results in **Table 3,** it is clear that the mass flow rate turns out to be the only significant factor since it has a high F-value of 282.73 and a P-value of 0.004 ($p<0.05$). In addition, the Adjusted Sum of Squares (Adj SS) corresponding to flow rate (0.102907) is almost similar to the Total Sum of Squares (0.103470), showing that it explains about 99.5% of the variation in the data. This shows the dominance of this parameter over the other parameters. On the contrary, the channel height (high) and absorber material have high p-values of 0.692 and 0.908, respectively, which show that their effects are not significant and can be due to random variation. In addition, the low value of the error term also indicates that the model developed is accurate in explaining the system behavior.

Table 3. Analysis of variance (ANOVA) for process parameters.

Exp. No	Source	DF	Adj SS	Adj MS	F-Value	P-Value
1	High	2	0.00016	8.1E-05	0.45	0.692
2	Flow Rate	2	0.10291	0.05145	282.73	0.004
3	Material	2	3.7E-05	1.8E-05	0.1	0.908
4	Error	2	0.00036	0.00018		
5	Total	8	0.10347			

Such a great significance of mass flow rate can be explained by its direct impact on the airflow velocity, which increases the convective heat transfer coefficient and enhances heat transfer from the absorber plate to the flowing air. On the contrary, the insignificant role of channel height and absorber material indicates that the system performance is primarily governed by convection within the investigated operating range.
From **Table 4**, it is possible to conclude that the accuracy and reliability of the developed model are very high, meaning the high accuracy of modeling. The coefficient of determination R-sq (99.65%) means that almost all the variability in the response variable is caused by the model. It is additionally supported by the adjusted R-sq (98.59%), which is close to R-sq. It means that the model performance does not depend on any unnecessary terms, but it is affected only by the significance of the main parameter, which is the mass flow rate. Moreover, the predicted R-sq value (92.88%) is consistent with the adjusted R-sq. Thus, one can state that the model retains its high performance even when applied to new data. Finally, the relatively low value of standard error (S=0.0134902) confirms that there is no great dispersion between experimental and predicted values.

Table 4. Model summary for statistical reliability analysis

No	S	R-sq	R-sq(adj)	R-sq(pred)
1	0.0135	99.65%	98.59%	92.88%

$$\eta = 0.42684 - 0.00462(High30) - 0.00102(High50) + 0.00563(High70) - 0.15016(\dot{m}\,0.01) + 0.05957(\dot{m}\,0.07) + 0.09058(\dot{m}\,0.15) - 0.00189(Aluminum) - 0.00092(Copper) + 0.00280(Steel) \quad (8)$$

The percent contribution of each factor to the response is presented in **Table 5**. As clearly observed, mass flow rate is the factor that controls the behavior of the system, with the largest contribution amounting to about 99.46%. In addition, channel height and absorber material have insignificant contributions since they contribute less than 0.2% to the overall effect. This again proves the results of the ANOVA analysis, which clearly indicated that mass flow rate is the controlling parameter in the system.

Table 5. Percentage contribution of factors to the response variable.

No	Factor	Significant Percentage %
1	High	0.156567
2	Flow Rate	99.45588
3	Material	0.035759
4	error	0.351793

Although the ANOVA results indicate that the absorber plate material contributes less than 0.2% to the thermal efficiency, it was intentionally included as one of the optimization factors to quantitatively evaluate its influence under identical operating conditions. Copper, aluminium, and steel were selected because they are among the most widely used engineering materials for solar absorber plates and exhibit significantly different thermal conductivities. Moreover, only a limited number of previous studies have quantitatively compared these materials under identical operating conditions using an integrated CFD–Taguchi–ANOVA approach. Including absorber material in the optimization process provides a quantitative assessment of its relative importance compared with other design and operating parameters. The results demonstrate that the air mass flow rate is the dominant parameter governing the collector thermal performance, whereas the effects of channel height and absorber material are statistically insignificant within the investigated operating range. This finding provides useful engineering guidance, indicating that lower-cost materials may be selected without significantly compromising the thermal efficiency of the collector.

Fig. 10 shows that as the flow rate increases, the thermal efficiency also increases, especially for flow rate values that exceed 0.10. On the other hand, variations in channel height insignificantly affect the response. The nearly vertical contour bands indicate that thermal efficiency is much more sensitive to variations in mass flow rate than to channel height. This behavior is consistent with the ANOVA results, which identified the mass flow rate as the dominant factor controlling the collector performance. Therefore, there is an operational window within which the peak efficiency can be achieved despite significant variations in channel height, provided that the mass flow rate is maintained at higher values.

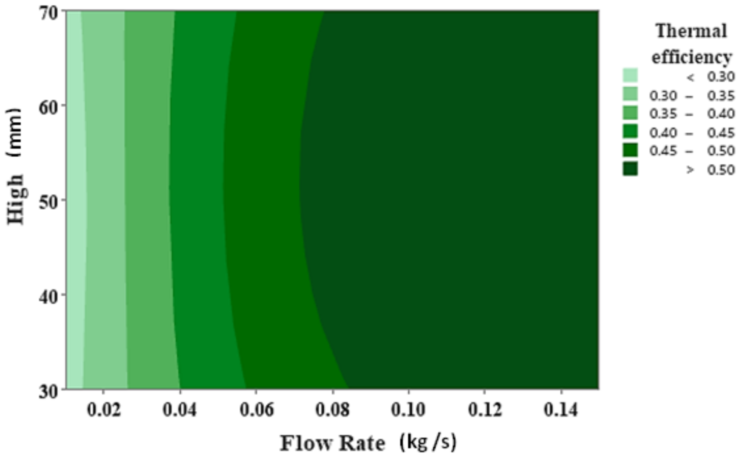

Figure 10. Contour plot for thermal efficiency against high (mm) and flow rate (kg/s)

As shown in **Fig. 11**, by the Taguchi method, the optimal combination of parameters was found to be a high channel dimension (70/30 mm), high mass flow rate (0.15 kg/s), and steel absorber material. Since this combination of parameters did not exist in the initial L9 orthogonal array, a confirmatory simulation was done in ANSYS to verify its effectiveness. The thermal efficiency value calculated was 0.5305, which is almost equal to the maximum thermal efficiency obtained in the L9 array (0.53112, copper absorber material). This similarity proves that the Taguchi method gives accurate results, and similar results can be obtained with steel absorber material.

The negligible influence of the absorber material can be attributed to the dominant role of convective heat transfer in the present collector configuration. Although copper, aluminum, and steel exhibit significantly different thermal conductivities, the absorber plate is relatively thin, resulting in a very low conduction thermal resistance. Consequently, heat is rapidly distributed throughout the absorber regardless of the material type. Under these conditions, the overall thermal resistance of the collector is governed primarily by the convective resistance between the absorber surface and the flowing air rather than by conduction through the absorber plate. Therefore, increasing the air mass flow rate enhances the convective heat transfer coefficient and becomes the dominant mechanism controlling the collector thermal efficiency, whereas variations in absorber thermal conductivity produce only a marginal effect within the investigated operating range.

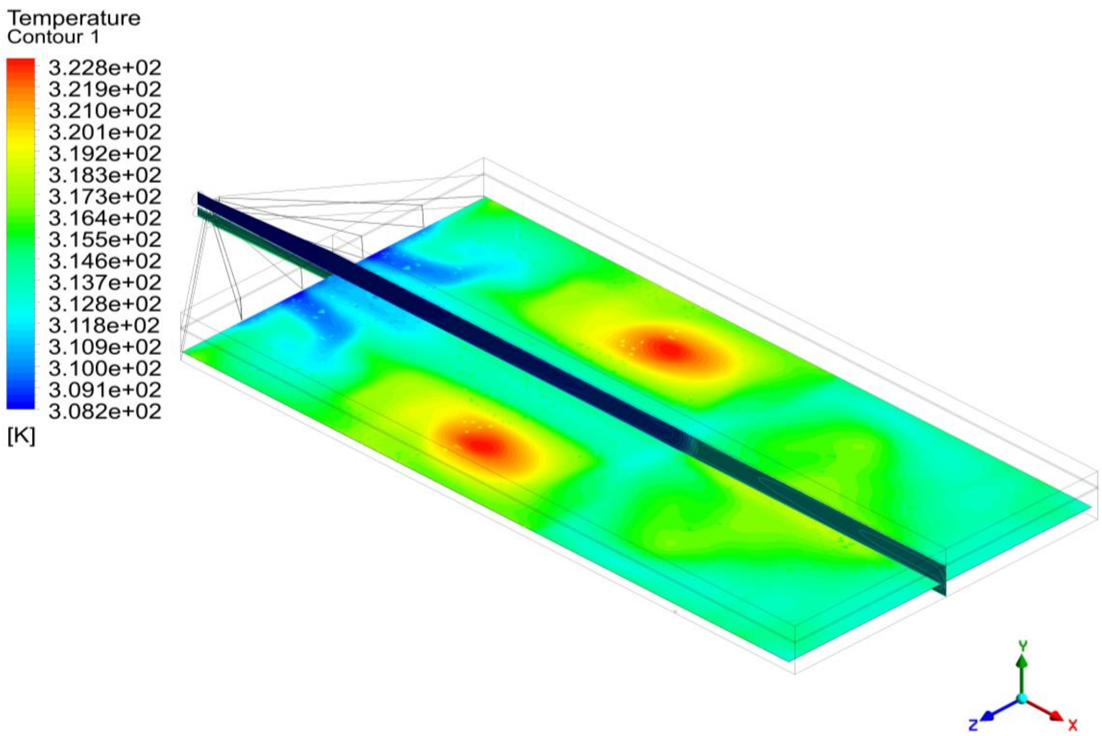

Figure 11. Contour plot of temperature for the optimum case (10) thermal efficiency.

4. REGRESSION MODEL INTERPRETATION

From the regression analysis, it is clear that:

- Coefficients for flow rate are dominant and positive, especially at 0.15 kg/s with a coefficient of 0.09058, confirming that flow rate is the most influential parameter affecting thermal efficiency.
- Coefficients for height are very small, ranging from −0.00462 to 0.00563, confirming their weak influence.
- Coefficients for absorber material are also very small, ranging from −0.00189 to 0.00280, indicating their negligible effect on the collector thermal efficiency.

This suggests that there is a linear relationship between the system behavior and the flow rate, with little dependence on the other parameters studied.

5. CONCLUSIONS

The present study numerically investigated the thermal performance of a double-pass counter-flow solar air collector using a three-dimensional CFD model integrated with the Taguchi optimization method and ANOVA statistical analysis. Based on the obtained results, the following conclusions can be drawn:

1. The maximum thermal efficiency was 0.53112, while the optimum thermal efficiency of 0.5305, demonstrating the reliability of the Taguchi optimization approach.
2. ANOVA showed that the air mass flow rate was the dominant parameter affecting thermal efficiency, contributing 99.46% of the total variation, while the effects of channel height and absorber material were insignificant.
3. Increasing the air mass flow rate from 0.01 to 0.15 kg/s improved the thermal efficiency by approximately 90.3%.
4. Although copper, aluminum, and steel have significantly different thermal conductivities, the absorber material contributed less than 0.2% to the overall thermal efficiency.
5. The developed regression model demonstrated excellent predictive capability with an R^2 value of 99.65%.
6. From an engineering perspective, the results indicate that optimizing the air mass flow rate is considerably more effective than changing the absorber material.

NOMENCLATURE

Symbol	Description	Symbol	Description
A	Area, m^2.	V	Velocity magnitude, m/s.
C_p	Specific heat capacity of air, J/kg.K.	W	Collector width, mm.
E	Total energy, J/kg.	**Greek Symbols**	
g_a	Air gap, mm.	δ	Kronecker delta /unit tensor.
G_k	Generation of turbulent kinetic energy.	ε	Turbulent dissipation rate, m^2/s^3.
h	Convective heat transfer coefficient, $W/m^2.K$.	η	Thermal efficiency, %.
H	Channel height, mm.	μ	Dynamic viscosity, kg/m.s.
I	Solar radiation, W/m^2.	μ_t	Turbulent viscosity, Kg/m.s.
k	Thermal conductivity, W/m.K.	ρ	Density, Kg/m^3.
k_t	Turbulent kinetic energy, m^2/s^2.	$\bar{\bar{\tau}}$	Stress tensor.
L	Collector length, mm.	**Subscript**	
$\dot{m}$	Air mass flow rate, kg/s.	f	Fluid
P	Pressure, Pa.	in	Inlet
q	Heat flux, W/m^2.	out	Outlet
Q_u	Useful heat gain, W.	s	Solid
$Q_{u,Presen}$	Present useful heat gain, W.	u	useful
$Q_{u,ref}$	Reference useful heat gain, W.	**Abbreviation**	
T	Temperature, K.	CFD	Computational fluid dynamics
T_{in}	Inlet air temperature, K.	SAH	Solar air heater
T_{out}	Outlet air temperature, K.	DCSAH	Double-pass counter flow solar air heater.
u	Air velocity, m/s.		

Acknowledgements

The authors would like to express their sincere appreciation to the supervisors and the Department of Energy Engineering, University of Baghdad, for their valuable guidance and continuous support throughout this work.

Credit Authorship Contribution Statement

Hussein Muwafaq M. Ali: Conceptualization, Methodology, Software, Numerical Simulation, Validation, Formal analysis, Investigation, Data curation, Writing – original draft, Writing – review & editing. Hussein K. Jobair: Methodology, Investigation, Supervision, Technical guidance, Validation, Writing – review & editing. Oday Ibraheem Abdullah: Methodology, Investigation, Supervision, Technical guidance, Writing – review & editing.

Declaration of Competing Interest

The authors declare that they have no known competing financial interests or personal relationships that could have appeared to influence the work reported in this paper.

REFERENCES

Aharwal, K.R., Gandhi, B.K., and Saini, J.S., 2009. Heat transfer and friction characteristics of solar air heater ducts having integral inclined discrete ribs on absorber plate. *International Journal of Heat and Mass Transfer*, 52(25–26), pp. 5970–5977. http://doi.org/10.1016/j.ijheatmasstransfer.2009.05.032

Alam, T., and Kim, M.H., 2016. Numerical study on thermal hydraulic performance improvement in solar air heater duct with semi ellipse shaped obstacles. *Energy*, 112, pp. 588–598. http://dx.doi.org/10.1016/j.energy.2016.06.105

Arpaci, V.S., and Larsen, P. S., 1984. *Convection Heat Transfer*. Prentice Hall, Upper Saddle River, NJ.

Batchelor, G.K., 1967. *An Introduction to Fluid Dynamics*. Cambridge University Press, Cambridge, UK.

Bhagoria, J.L., Saini, J.S., and Solanki, S.C., 2002. Heat transfer coefficient and friction factor correlations for rectangular solar air heater duct having transverse wedge shaped rib roughness on the absorber plate. *Renewable Energy*, 25(3), pp. 341–369. https://doi.org/10.1016/S0960-1481(01)00057-X

Bisnovatyi-Kogan, G.S., and Lovelace, R.V.E., 2001. Advective accretion disks and related problems including magnetic fields. *New Astronomy Reviews*, 45(11–12), pp. 663–742. https://doi.org/10.1016/S1387-6473(01)00146-4

Chand, S., Chand, P. , and Ghritlahre, H.K., 2022. Thermal performance enhancement of solar air heater using louvered fins collector. *Solar Energy*, 239, pp. 10–24. https://doi.org/10.1016/j.solener.2022.04.046

Choi, H.U., and Choi, K.H., 2020. CFD analysis on the heat transfer and fluid flow of solar air heater having transverse triangular block at the bottom of air duct. *Energies*, 13(5), P. 1099. https://doi.org/10.3390/en13051099

Gill, R.S., Hans, V.S., and Singh, R.P., 2021. Optimization of artificial roughness parameters in a solar air heater duct roughened with hybrid ribs. *Applied Thermal Engineering*, 191, P. 116871. https://doi.org/10.1016/j.applthermaleng.2021.116871.

Gupta, D., Solanki, S.C., and Saini, J.S., 1993. Heat and fluid flow in rectangular solar air heater ducts having transverse rib roughness on absorber plates. *Solar Energy*, 51(1), pp. 31–37. https://doi.org/10.1016/0038-092X(93)90039-Q.

Haldar, A., Varshney, L., and Verma, P., 2022. Effect of roughness parameters on performance of solar air heater having artificial wavy roughness using CFD. *Renewable Energy*, 184, pp. 266–279. https://doi.org/10.1016/j.renene.2021.11.088.

Hamad, R.F., Alshukri, M.J., Eidan, A.A., and Alsabery, A.I., 2023. Numerical investigation of heat transfer augmentation of solar air heater with attached and detached trapezoidal ribs. *Energy Reports*, 10, pp. 123–134. https://doi.org/10.1016/j.egyr.2023.06.031.

Hans, V.S., Saini, R.P., and Saini, J.S., 2010. Heat transfer and friction factor correlations for a solar air heater duct roughened artificially with multiple V-ribs. *Solar Energy*, 84(6), pp. 898–911. https://doi.org/10.1016/j.solener.2010.02.004.

Hussein, N.F., Ahmed, S.T., and Ekaid, A.L., 2023. Thermal performance of double pass solar air heater with tubular solar absorber. *International Journal of Renewable Energy Development*, 12(1). https://doi.org/10.14710/ijred.2023.46328.

Jobair, H.K., and Nima, M.A., 2025. Experimental and numerical investigation of a double pass solar air heater provided with porous absorber plate for drying applications. *Special Topics and Reviews in Porous Media*, 16(1). https://doi.org/10.1615/specialtopicsrevporousmedia.2024049482.

Karwa, R., Solanki, S.C., and Saini, J.S., 1999. Heat transfer coefficient and friction factor correlations for the transitional flow regime in rib-roughened rectangular ducts. *International Journal of Heat and Mass Transfer*, 42(9), pp. 1597–1615. https://doi.org/10.1016/S0017-9310(98)00252-X.

Kumar, R., Sharma, A., Goel, V., Sharma, R., Sethi, M., and Tyagi, V.V., 2023. An experimental investigation of new roughness patterns (dimples with alternative protrusions) for the performance enhancement of solar air heater. *Renewable Energy*, 211, pp. 964–974. https://doi.org/10.1016/j.renene.2023.04.111.

Layek, A., Saini, J.S., and Solanki, S.C., 2007. Second law optimization of a solar air heater having chamfered rib–groove roughness on absorber plate. *Renewable Energy*, 32(12), pp. 1967–1980. https://doi.org/10.1016/j.renene.2006.11.005.

Misra, R., Singh, J., Jain, S.K., Faujdar, S., Agrawal, M., Mishra, A., and Goyal, P. K., 2020. Prediction of behavior of triangular solar air heater duct using V-down rib with multiple gaps and turbulence promoters as artificial roughness: A CFD analysis. *International Journal of Heat and Mass Transfer*, 162, P. 120376. https://doi.org/10.1016/j.ijheatmasstransfer.2020.120376.

Nagaraj, M., Reddy, M.K., Honnesara Sheshadri, A.K., and Karanth, K.V., 2022. Numerical analysis of an aerofoil fin integrated double pass solar air heater for thermal performance enhancement. *Sustainability*, 15(1), P. 591. https://doi.org/10.3390/su15010591.

Panda, S., and Kumar, R., 2021. A review on heat transfer enhancement of solar air heater using various artificial roughed geometries. *Journal of Advanced Research in Fluid Mechanics and Thermal Sciences*, 89(1), pp. 92–133. https://doi.org/10.37934/arfmts.89.1.92133.

Parsa, H., Saffar-Avval, M., and Hajmohammadi, M.R., 2021. 3D simulation and parametric optimization of a solar air heater with novel staggered cuboid baffles. *International Journal of Mechanical Sciences*, 205, P. 106607. https://doi.org/10.1016/j.ijmecsci.2021.106607.

Patel, Y.M., Jain, S.V., and Lakhera, V.J., 2020. Thermo-hydraulic performance analysis of a solar air heater roughened with reverse NACA profile ribs. *Applied Thermal Engineering*, 170, P. 114940. https://doi.org/10.1016/j.applthermaleng.2020.114940.

Prasad, K., and Mullick, S.C., 1983. Heat transfer characteristics of a solar air heater used for drying purposes. *Applied Energy*, 13(2), pp. 83–93. https://doi.org/10.1016/0306-2619(83)90001-6.

Ramani, B.M., Gupta, A., and Kumar, R., 2010. Performance of a double pass solar air collector. *Solar Energy*, 84(11), pp. 1929–1937. https://doi.org/10.1016/j.solener.2010.07.007.

Sahu, M.M., and Bhagoria, J.L., 2005. Augmentation of heat transfer coefficient by using 90° broken transverse ribs on absorber plate of solar air heater. *Renewable Energy*, 30(13), pp. 2057–2073. https://doi.org/10.1016/j.renene.2004.10.016.

Saini, S.K., and Saini, R.P., 2008. Development of correlations for Nusselt number and friction factor for solar air heater with roughened duct having arc-shaped wire as artificial roughness. *Solar Energy*, 82(12), pp. 1118–1130. https://doi.org/10.1016/j.solener.2008.05.010.

Saravanan, A., Murugan, M., Reddy, M.S., Ranjit, P. S., Elumalai, P. V., Kumar, P., and Sree, S.R., 2021. Thermo-hydraulic performance of a solar air heater with staggered C-shape finned absorber plate. International Journal of Thermal Sciences, 168, P. 107068. https://doi.org/10.1016/j.ijthermalsci.2021.107068.

Shaheed, R., Mohammadian, A., and Kheirkhah Gildeh, H., 2019. A comparison of standard k–ε and realizable k–ε turbulence models in curved and confluent channels. *Environmental Fluid Mechanics*, 19(2), pp. 543–568. https://doi.org/10.1007/s10652-018-9637-1.

Singh, I., and Singh, S., 2018. CFD analysis of solar air heater duct having square wave profiled transverse ribs as roughness elements. *Solar Energy*, 162, pp. 442–453. https://doi.org/10.1016/j.solener.2018.01.019.

Singh, S., Singh, B., Hans, V.S., and Gill, R.S., 2015. CFD investigation on Nusselt number and friction factor of solar air heater duct roughened with non-uniform cross-section transverse rib. *Energy*, 84, pp. 509–517. https://doi.org/10.1016/j.energy.2015.03.015.

Srivastava, A., Chhaparwal, G.K., and Sharma, R.K., 2020. Numerical and experimental investigation of different rib roughness in a solar air heater. *Thermal Science and Engineering Progress*, 19, P. 100576. https://doi.org/10.1016/j.tsep.2020.100576.

Varun, Saini, R.P., and Singal, S.K., 2007. A review on roughness geometry used in solar air heaters. *Solar Energy*, 81(11), pp. 1340–1350. https://doi.org/10.1016/j.solener.2007.01.017.

Yadav, A.S., and Bhagoria, J.L., 2013. A CFD analysis of a solar air heater having triangular rib roughness on the absorber plate. *International Journal of ChemTech Research*, 5(2), pp. 964–971.

Yadav, S., and Kaushal, M., 2013. Nusselt number and friction factor correlations for solar air heater duct having protrusions as roughness elements on absorber plate. *Experimental Thermal and Fluid Science*, 44, pp. 34–41. https://doi.org/10.1016/j.expthermflusci.2012.05.011.

دراسة عددية للأداء الحراري لمجمع هواء شمسي ذي لوح مسطح مزدوج التدفق المعاكس بأستخدام طريقة تاغوشي

حسين موفق محمدعلي[1، *]، عدي أبراهيم عبدالله[1، 2، 3]، حسين خلف جبير[1]

[1]قسم هندسة الطاقة، كلية الهندسة، جامعة بغداد، بغداد، العراق
[2] قسم الهندسة الميكانيكية، كلية الهندسة، جامعة الخليج، سند، البحرين
[3] قسم هندسة النفط، كلية الهندسة، جامعة الناجي، بغداد، العراق

الخلاصة

تُستخدم مُجمِّعات الهواء الشمسية على نطاق واسع في الصناعات والزراعة نظرًا لبساطة تصميمها وجدواها الاقتصادية، إلا أن خصائص أدائها الحراري محدودة بسبب عدم كفاية التبادل الحراري بالحمل بين السطح الممتص وتدفق الهواء. في هذه الدراسة، تم إجراء بحث عددي وتحسين لخصائص الأداء الحراري لمُجمِّع الهواء الشمسي ذي اللوح المسطح ذي التدفق المعاكس والممر المزدوج باستخدام طريقة CFD-Taguchi. تم نمذجة الحرارة وتدفق الهواء في ظل ظروف الحمل القسري في برنامج ANSYS باستخدام نمذجة ثلاثية الأبعاد للحالة المستقرة (CFD). دُرست عوامل رئيسية مثل معدل تدفق الكتلة (0.01−0.07−0.15 كجم/ث)، وتكوينات ارتفاع القناة، وخصائص المواد (النحاس والألومنيوم والفولاذ). باستخدام تحليل تاغوشي وتقنية ANOVA، تم الحصول على توليفة مثلى من المعلمات لتحسين الخصائص الحرارية. أظهرت نتائج المحاكاة أن أعلى كفاءة مُحققة بلغت 0.531، حيث تبيّن أن معدل تدفق الكتلة هو العامل المهيمن الذي يُفسّر 99.46% من التأثيرات الكلية. يُمكن تحقيق كفاءة أعلى بزيادة معدل التدفق نتيجةً لزيادة عملية الحمل الحراري؛ إلا أن زيادة معدل تدفق الكتلة تُقلّل من درجة حرارة مخرج الهواء بسبب قصر فترة التعرض. كان تأثير ارتفاع القناة ونوع المادة ضئيلاً للغاية (أقل من 0.2%). تم التحقق من صحة النموذج النظري باستخدام بيانات منشورة، وبلغت نسبة الخطأ القصوى 6.65%. من هذه الدراسة، يتضح أن التركيز على إدارة تدفق الهواء بشكل سليم أهم من اختيار المادة المناسبة.

الكلمات المفتاحية: مادة ماصة، ديناميكا الموائع الحسابية، جامع الهواء، طريقة تاغوشي، الكفاءة الحرارية.